Transit timing variations of AU Microscopii b and c

Gy. M. Szabó, Z. Garai, A. Brandeker, D. Gandolfi, T. G. Wilson, A. Deline, G. Olofsson, A. Fortier, D. Queloz, L. Borsato, et al.

▶ **To cite this version:**

Gy. M. Szabó, Z. Garai, A. Brandeker, D. Gandolfi, T. G. Wilson, et al.. Transit timing variations of AU Microscopii b and c. Astronomy & Astrophysics - A&A, 2022, 659, ⟨10.1051/0004-6361/202243076⟩. ⟨insu-03705368⟩

HAL Id: insu-03705368

https://insu.hal.science/insu-03705368v1

Submitted on 27 Jun 2022

HAL is a multi-disciplinary open access archive for the deposit and dissemination of scientific research documents, whether they are published or not. The documents may come from teaching and research institutions in France or abroad, or from public or private research centers.

L'archive ouverte pluridisciplinaire **HAL**, est destinée au dépôt et à la diffusion de documents scientifiques de niveau recherche, publiés ou non, émanant des établissements d'enseignement et de recherche français ou étrangers, des laboratoires publics ou privés.

HAL Authorization

A&A 659, L7 (2022)
https://doi.org/10.1051/0004-6361/202243076
© ESO 2022

Astronomy & Astrophysics

LETTER TO THE EDITOR

Transit timing variations of AU Microscopii b and c*

Gy. M. Szabó[1,2], Z. Garai[1,2,3], A. Brandeker[4], D. Gandolfi[5], T. G. Wilson[6], A. Deline[7], G. Olofsson[4], A. Fortier[8,9], D. Queloz[7,10], L. Borsato[11], F. Kiefer[12], A. Lecavelier des Etangs[12], M. Lendl[7], L. M. Serrano[5], S. Sulis[13], S. Ulmer Moll[7], V. Van Grootel[14], Y. Alibert[8], R. Alonso[15,16], G. Anglada[17,18], T. Bárczy[19], D. Barrado y Navascues[20], S. C. C. Barros[21,22], W. Baumjohann[23], M. Beck[7], T. Beck[8], W. Benz[8,9], N. Billot[7], A. Bonfanti[23], X. Bonfils[24], C. Broeg[8,9], J. Cabrera[25], S. Charnoz[26], A. Collier Cameron[6], Sz. Csizmadia[25], M. B. Davies[27], M. Deleuil[13], L. Delrez[14,28], O. Demangeon[21,22], B.-O. Demory[9], D. Ehrenreich[7], A. Erikson[25], L. Fossati[23], M. Fridlund[29,30], M. Gillon[28], M. Güdel[31], K. Heng[9,32], S. Hoyer[13], K. G. Isaak[33], L. L. Kiss[34,47], J. Laskar[35], C. Lovis[7], D. Magrin[11], P. F. L. Maxted[36], M. Mecina[37], V. Nascimbeni[11], R. Ottensamer[37], I. Pagano[38], E. Pallé[15], G. Peter[39], G. Piotto[11,40], D. Pollacco[32], R. Ragazzoni[11,40], N. Rando[41], H. Rauer[25,42,43], I. Ribas[17,18], N. C. Santos[21,22], M. Sarajlic[8], G. Scandariato[38], D. Ségransan[7], A. E. Simon[8], A. M. S. Smith[25], S. G. Sousa[21], M. Steller[23], N. Thomas[8], S. Udry[7], F. Verrecchia[44,45], N. Walton[46], and D. Wolter[25]

(Affiliations can be found after the references)

Received 10 January 2022 / Accepted 1 February 2022

ABSTRACT

Here we report large-amplitude transit timing variations (TTVs) for AU Microcopii b and c as detected in combined TESS (2018, 2020) and CHEOPS (2020, 2021) transit observations. AU Mic is a young planetary system with a debris disk and two transiting warm Neptunes. A TTV on the order of several minutes was previously reported for AU Mic b, which was suggested to be an outcome of mutual perturbations between the planets in the system. In 2021, we observed AU Mic b (five transits) and c (three transits) with the CHEOPS space telescope to follow-up the TTV of AU Mic b and possibly detect a TTV for AU Mic c. When analyzing TESS and CHEOPS 2020−2021 measurements together, we find that a prominent TTV emerges with a full span of ≥23 min between the two TTV extrema. Assuming that the period change results from a periodic process –such as mutual perturbations– we demonstrate that the times of transits in the summer of 2022 are expected to be 30−85 min later than predicted by the available linear ephemeris.

Key words. planets and satellites: fundamental parameters – planets and satellites: individual: AU Mic b and c

1. Introduction

AU Microscopii is the epitome of a young planetary system, where planets orbit a late-type star, with possible star–planet interactions. Its age is estimated to be 22 Myr (Mamajek & Bell 2014), and as a β Pictoris Moving Group (Torres et al. 2006) member, it has a dynamical trace-back age of 18.5 ± 2 Myr (Miret-Roig et al. 2020), making it one of the youngest known exoplanet systems. AU Mic hosts two transiting warm Neptunes near mean-motion resonances (Plavchan et al. 2020). Recurrent spot occultations along the transit chord are observed thanks to a 7:4 spin–orbit commensurability between the orbital period of AU Mic b and the stellar rotation (Szabó et al. 2021).

Eight transits of AU Mic b have been published so far. TESS (Ricker et al. 2014) observed two and three transits in 2018 and 2020, respectively (Gilbert et al. 2021), and CHEOPS (Benz et al. 2021) observed three transits in 2020 (previously reported in Szabó et al. 2021). All published data on AU Mic c so far come from TESS, covering one transit in 2018 and two in 2020 (Plavchan et al. 2020; Gilbert et al. 2021). The previous observations led to somewhat inconsistent period estimates for AU Mic b (with a scatter significantly larger than expected from the estimated timing uncertainty), which has recently been suggested to reflect TTVs on the order of 80 s (reported by Gilbert et al. 2021) or 3 min (by Martioli et al. 2021).

Here we present new photometric observations of AU Mic b and AU Mic c carried out with the CHEOPS space telescope from July through September, 2021. We describe the observations and data-processing methods in Sect. 2 and present the results in Sect. 3.

2. Observations and data processing

During the 2021 opposition, we observed five transits of AU Mic b and three transits of AU Mic c. Four of the five AU Mic b transits and two of the AU Mic c transits are appropriate for transit timing analysis. For the fifth AU Mic b transit (21-09-25), both the ingress and egress are missing because of gaps in the data. These transits will be analyzed in a forthcoming publication. Similarly to the third 2020 observation with CHEOPS, we used short exposure times of 3 s to better resolve possible flares. The brightness of the star (V = 8.6 mag and *Gaia* G = 7.843 mag; Kiraga 2012; Gaia Collaboration 2018) ensured an adequate signal despite the short exposures. See Table 1 for the observations log. In the CHEOPS Proposal Handling Tool,

* The CHEOPS data are only available at the CDS via anonymous ftp to cdsarc.u-strasbg.fr (130.79.128.5) or via http://cdsarc.u-strasbg.fr/viz-bin/cat/J/A+A/659/L7

Table 1. Logs of AU Mic observations by CHEOPS included in this Letter.

Visit ID	Start date (2021)	End date (2021)	File key	CHEOPS product	Integ. time (s)	Co-added exposures	Num. of frames
AU Mic b 21-07-26	07-26 11:27:13	07-26 22:34:04	PR100010_TG003001	Subarray	42	3 s × 14	669
				Imagettes	3	–	9366
AU Mic c 21-08-09	08-09 04:59:15	08-09 19:37:47	PR100010_TG003401	Subarray	42	3 s × 14	1029
				Imagettes	3	–	14 406
AU Mic b 21-08-12	08-12 08:25:41	08-12 19:53:00	PR100010_TG003601	Subarray	42	3 s × 14	839
				Imagettes	3	–	11 746
AU Mic c 21-08-28	08-28 02:09:13	08-28 16:35:03	PR100010_TG003402	Subarray	42	3 s × 14	907
				Imagettes	3	–	12 698
AU Mic b 21-08-29	08-29 05:17:41	08-29 16:44:59	PR100010_TG003701	Subarray	42	3 s × 14	667
				Imagettes	3	–	9338
AU Mic b 21-09-06	09-06 17:38:41	09-07 05:05:59	PR100010_TG003101	Subarray	42	3 s × 14	643
				Imagettes	3	–	9002

Notes. The time notation follows the ISO-8601 convention. The File key supports the fast identification of the observations in the CHEOPS archive.

we set up observation windows with an observation length covering seven (AU Mic b) and nine CHEOPS orbits (AU Mic c), with one CHEOPS orbit lasting 98.77 min. We centered each visit at the predicted mid-transit time and observed for the entire transit duration, adding at least 1.5 CHEOPS orbits on each side in order to have a reasonably long out-of-transit baseline. The efficiency of the observations varied between 55% and 90%.

The sub-array frames were automatically processed with the CHEOPS Data Reduction Pipeline (DRP; Hoyer et al. 2020). In addition to the sub-arrays, there are imagettes available for each exposure. The imagettes are images of 30 pixels in radius centered on the target and do not need to be co-added before download owing to their smaller size. We used a tool specifically developed for photometric extraction of imagettes using point-spread function (PSF) photometry, PIPE (PSF imagette photometric extraction; for more details of how it was applied to AU Mic data, we refer to Szabó et al. 2021). The PIPE photometry has a signal-to-noise ratio (S/N) comparable to that of DRP photometry, but has a lower cadence, allowing better identification of flares (Szabó et al. 2021).

In this Letter, we analyze the PIPE reduction averaged to 15 s cadence for better S/N of individual points. The data reduced with both DRP and PIPE are available at the CDS.

2.1. Pre-processing of the light curves

Due to the rotation of the host star, the stellar brightness slowly varied during the observations. This was removed by fitting a fourth-order polynomial to the out-of-transit light curve segments before starting the analysis.

Because flares can severely bias the transit model, we masked them out during the transits before the modeling. The longest flare with at least three major, complex humps occurred around the ingress phase of the CHEOPS 21-07-26 visit, and only the egress of this transit could be kept for further analysis. A shorter lasting flare was observed during the transits of the CHEOPS 21-08-29 and CHEOPS 21-09-23 visits, which nevertheless did not affect the ingress and egress phases.

We show the raw CHEOPS light curves after a subtraction of the polynomial slow-trend model and the image synthesis model of background contamination in Fig. A.1. We note that the segments of light curves contaminated by flares (in smaller dots in the figure) were omitted from the fit.

A visual inspection of the light curve led us to conclude that the level of red noise is not negligible. A quantitative analysis showed that the residuals after fitting the transits on the 2021 light curves are on average 280 ppm, higher than the 125 ppm residuals we found in the 2020 data (see also Fig. 1 and its discussion). The increasing red noise can be attributed to an increased stellar activity in 2021 compared to 2020. The increasing activity between 2018 and 2020 was also observed by TESS (Gilbert et al. 2021; Martioli et al. 2021). The adverse effects of increased activity are stronger for AU Mic c transits because of their shallowness, making the transit parameters more sensitive to red noise. The changing spot coverage of the star leads to a bias in the planet size ($R_p/R_\star$) parameter as well (see Tables 2 and 3 and the discussions that follow them).

Because of the spin–orbit commensurability (Szabó et al. 2021) of AU Mic b, the transits 21-07-26 and 21-08-29 are observed in front of the same stellar longitude. This longitude also coincides with the CHEOPS 20-08-21 and CHEOPS 20-09-24 observations shown in Szabó et al. (2021), but the change in the spot map does not allow a direct comparison between the years.

The phased transit light curves of both AU Mic b and AU Mic c are shown in Fig. 1. In both panels of this figure, the period P and epoch T_c of the transit times have been adopted from publications based on 2018−2020 data (AU Mic b and c: Martioli et al. 2021; Gilbert et al. 2021, respectively) to reflect the dramatic shift of the transits in reference to these linear ephemeris. The mid-transit of AU Mic b is shifted toward the positive phase coordinates, and a slight shift toward negative values is suspected in the case of AU Mic c. This is an impressive representation of how much the behavior of both planets changed within less than a year.

Both panels of Fig. 1 show the CHEOPS datasets without masking out the flares. In the case of AU Mic b, we see prominent anomalies mostly during the ingress phase and the start of the transit floor (around 0.00 phase coordinate according to the phase definition in Fig. 1). The ingress phase of the 21-07-26 transit is shallower than the other ones, which is further evidence of a positive anomaly at around phase 0.008 which is due to a

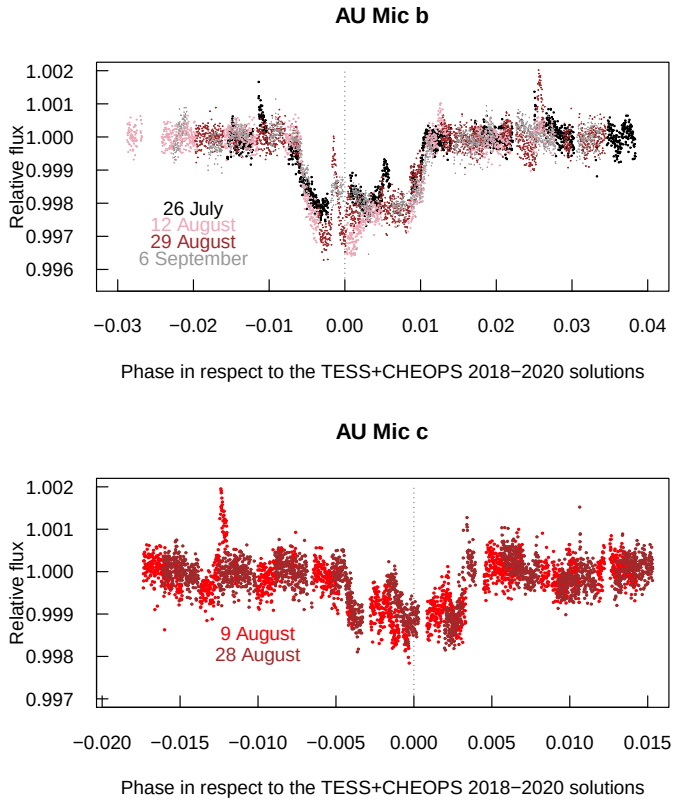

Fig. 1. Phased transit light curves of AU Mic b (*upper panel*) and AU Mic c (*lower panel*). The ordinate shows the orbital phase using the ephemeris of Szabó et al. (2021): $T_c = 2\,459\,041.28272$, $P = 8.462995$ in the case of AU Mic b, and $T_c = 2\,458\,342.2223$, $P = 18.859019$ in the case of AU Mic c. We highlight the huge phase shift of the 2021 transits with respect to the earlier linear ephemeris based on TESS and CHEOPS data from 2018 to 2020.

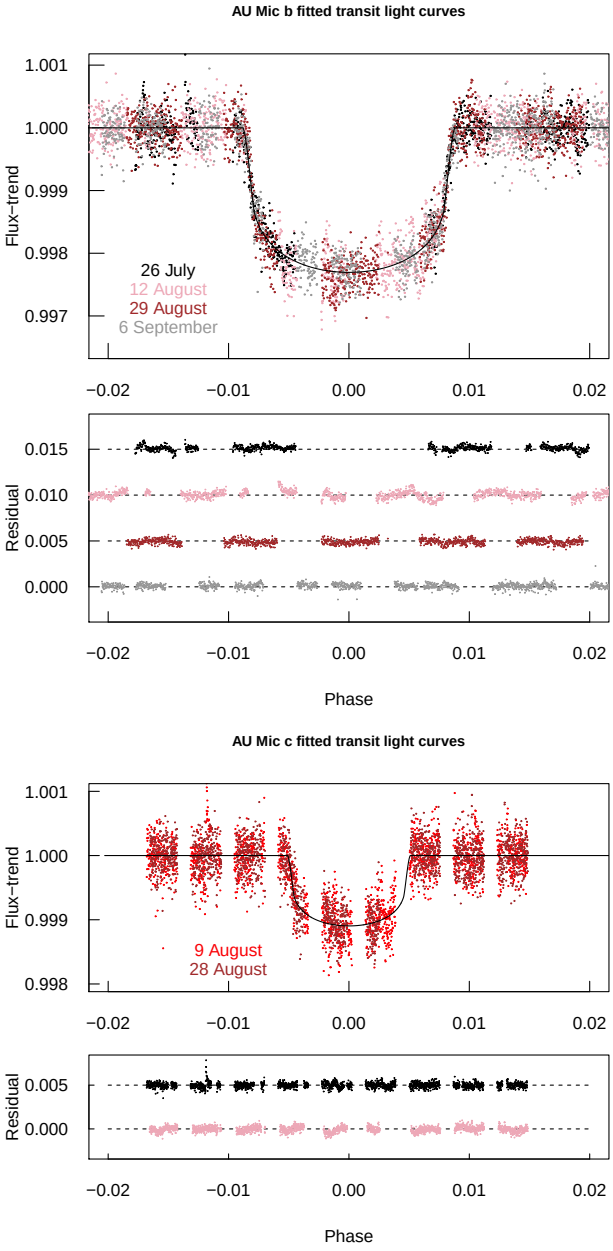

Fig. 2. Best-fit transit solutions of the four CHEOPS visits of AU Mic b (*upper panels*) and AU Mic c (*lower panels*) analyzed in this Letter, after omitting the flares during the transits. The phased points of the individual light curves are shown in light blue, and the binned light curve points of the individual transits are shown in dark blue. *Lower panel*: residuals observed at each individual visit. We highlight the increased variability of the light curve shape before the mid-transit of AU Mic b.

small flare. The 21-08-12 transit is significantly steeper than the other ones, which is likely the result of a different spot distribution (e.g., the beginning of the transit chord not covered by spots).

The 21-08-12 and 21-08-29 transits are exactly 3.5 stellar rotations apart and are therefore observed at opposite stellar longitudes. Interestingly, both of these transits have a "brightening" near the center of the transit, as if both of these transits happened in front of a spot. However, the presence of two large spots on opposite sides of the star is compatible with the rotation light curve of the star showing two minima during one rotation (Plavchan et al. 2020; Martioli et al. 2021; Szabó et al. 2021; Gilbert et al. 2021).

The phased transit curve of AU Mic c shows an unlucky coverage: the egress phase is within the data gaps in the case of both observations. There are also many residuals during the transits that are likely due to the presence of spot occultations. There is little resemblance between the residuals of the two planets. However, the impact parameter b is known to be different for the planets (Martioli et al. 2021; Gilbert et al. 2021), which means that the two transit chords map to different parts of the star. The observed residuals are consistent with this interpretation.

2.2. The transit model

After masking out the flares (as shown in Fig. A.1), we determined the transit parameters using the `pycheops` software module (Maxted et al. 2021). `pycheops` uses the `qpower2` transit model and the power-2 limb-darkening law (Maxted & Gill 2019); it calculates transit models of a spot-free star and a planet with a circular silhouette. The model parameters are the transit time (T_t), the transit depth parameter $D = (R_p/R_\star)^2$, the transit duration parameter $W = (R_\star/a)\sqrt{(1+k)^2 - b^2}/\pi$, and the impact parameter $b = a\cos(i)/R_\star$. The other system parameters can be derived from the above set; for example the transit duration expressed in hours as $W[h] = W \times P_i[h]$, where P_i is the instantaneous orbital period.

Table 2. Best-fitting parameters of AU Mic b.

	This Letter	P2020	M2021	Sz2021	G2021
$R_p/R_\star$	0.0433 ± 0.0017	0.0514 ± 0.0013	$0.0526^{+0.0003}_{-0.0002}$	0.0531 ± 0.0023	0.0512 ± 0.0020
$a/R_\star$	18.95 ± 0.35	$19.1^{+1.8}_{-1.6}$	$19.1^{+0.2}_{-0.4}$	19.24 ± 0.37	19.07
W [h]	3.51 ± 0.03	$3.50^{+0.63}_{-0.59}$	3.50 ± 0.08	3.48 ± 0.19	$3.56^{+0.60}_{-0.46}$
R_p [$R_\oplus$]	3.55 ± 0.13	4.29 ± 0.20	4.07 ± 0.17	4.36 ± 0.18	4.27 ± 0.17
a [AU]	0.0654 ± 0.0012	$0.066^{+0.007}_{-0.006}$	0.0645 ± 0.0013	0.0678 ± 0.0013	$0.0644^{+0.0056}_{-0.0054}$
b	0.17 ± 0.11	$0.16^{+0.14}_{-0.11}$	0.18 ± 0.11	0.09 ± 0.05	$0.26^{+0.13}_{-0.17}$

Notes. The parameters are compared to the results of Plavchan et al. (2020, P2020), Martioli et al. (2021, M2021), Szabó et al. (2021, Sz2021), and Gilbert et al. (2021, G2021).

Table 3. Best-fitting parameters of AU Mic c.

	This Letter	M2021	G2021
$R_p/R_\star$	0.0313 ± 0.0016	0.0395 ± 0.0011	$0.0340^{+0.0033}_{-0.0034}$
$a/R_\star$	28.8 ± 2.4	29 ± 3.0	$31.7^{+2.7}_{2.6}$
W [h]	4.29 ± 0.30	4.50 ± 0.80	$4.20^{+0.92}_{-0.67}$
R_p [$R_\oplus$]	2.56 ± 0.12	3.24 ± 0.16	$2.79^{+0.31}_{-0.30}$
a [AU]	0.0993 ± 0.0085	0.1101 ± 0.0022	$0.110^{+0.010}_{-0.010}$
b	0.58 ± 0.13	0.51 ± 0.21	$0.30^{+0.21}_{-0.20}$

Notes. The parameters are compared to the results of M2021 and G2021.

It is possible to fit more complex models to the observed transits that account for the presence of spots. In order to constrain the spot modeling, we performed ground-based observations simultaneously with the CHEOPS observations. We intend to publish this more complex modeling in a forthcoming paper, as the scope of this Letter is to primarily report the unexpectedly large TTVs, for which the standard modeling methods are sufficient (see Fig. 2).

The priors we used are listed in Table A.1 for both AU Mic b and AU Mic c. The stellar fundamental parameters were taken from SWEET-Cat (Sousa et al. 2018), which are the same parameters as in Plavchan et al. (2020). The noise model was calculated with `celerite` using the white-noise term `JitterTerm`($\log \sigma_w$) plus, optionally, a GP with kernel `SHOTerm`($\log \omega_0, \log S_0, \log Q$). The priors were identical to what we set up in Szabó et al. (2021).

The long-period trends of TTVs lead to the apparent change of the instantaneous orbital period. We fitted the instantaneous period as the P_i parameter to remove the linear trend of TTV in 2021. The actual mean orbital period, $P_{\rm mean}$, is the one that minimizes the scatter of the TTV. $P_{\rm mean}$ was determined by an $O-C$ analysis of mid-transit times (see Sect. 3, and also Tables A.2 and A.3).

3. Results

The best-fit transit parameters to 2021 CHEOPS observations are summarizsed in Tables 2 and 3, both for AU Mic b and AU Mic c. We compare our results to previous estimates in Plavchan et al. (2020), Szabó et al. (2021), Martioli et al. (2021), and Gilbert et al. (2021). In Szabó et al. (2021), we derived three sets of solutions using different solving algorithms (`pycheops` Maxted et al. 2021 and `TLCM` Csizmadia 2020), with resulting solutions that did not differ significantly from each other. As the present Letter uses the `pycheops` algorithm, we selected the `pycheops` solution in Szabó et al. (2021) for comparison with the 2021 observations.

3.1. Transit parameters

All parameters with the exception of $R_p/R_\star$ (and hence R_p) are compatible with all previous solutions in the literature. The most significant improvement of the present analysis is the increased precision of the transit duration, W, thanks to the combined precision of the four CHEOPS light curves, which have very good internal photometric accuracy.

The most relevant difference is observed in the $R_p/R_\star$ (and consequently, the R_p) planet radius parameters. In 2021, we observed smaller values than in 2018 and 2020, with a difference between the current and previous $R_p/R_\star$ estimates of 3.4σ. This is probably because the spot coverage of the stellar surface evolved between 2018 and 2021. It is known that spots along the transit chord decrease the transit depth, while unocculted spots increase it, and the naively determined $R_p/R_\star$ size parameter becomes inconsistent (Oshagh et al. 2013). Assuming that most spots are out of the transit chord, and therefore that spots increase the transit depth, Martioli et al. (2021) derived that in 2020, the actual diameter was overestimated by about 6% based on TESS data. Our result shows that the activity level increases between 2020 and 2021 while the transit depth decreases significantly, rather than being biased to larger values. The most simple explanation would be that spots of the host star are mostly on the transit chord of AU Mic b. We will discuss this possibility in detail in a forthcoming paper.

3.2. Large-amplitude TTVs

Both planets show a very prominent TTV. We complemented the CHEOPS (2020 and 2021) observations with mid-transit times of TESS data (2018 and 2020), and also the mid-transit time of the single *Spitzer* measurement fitted by Plavchan et al. (2020) (see the mid-transit times in Tables A.2 and A.3). Following Lithwick et al. (2012), the simplest form of a TTV can be described as a sinusoidal function with amplitude A and superperiod p, which are complicated functions of the exoplanet system parameters. Therefore,

$$O-C = A \sin\left(2\pi \frac{T_t}{p} + \phi\right) + c_1 T_t + c_2, \quad (1)$$

where T_t are individual transit times, and ϕ, c_1, and c_2 are free parameters determined by the selection of the time coordinate and the trial orbital period. We derive the mean orbital period $P_{\rm mean}$ and T_c, while demanding the elimination of the constant

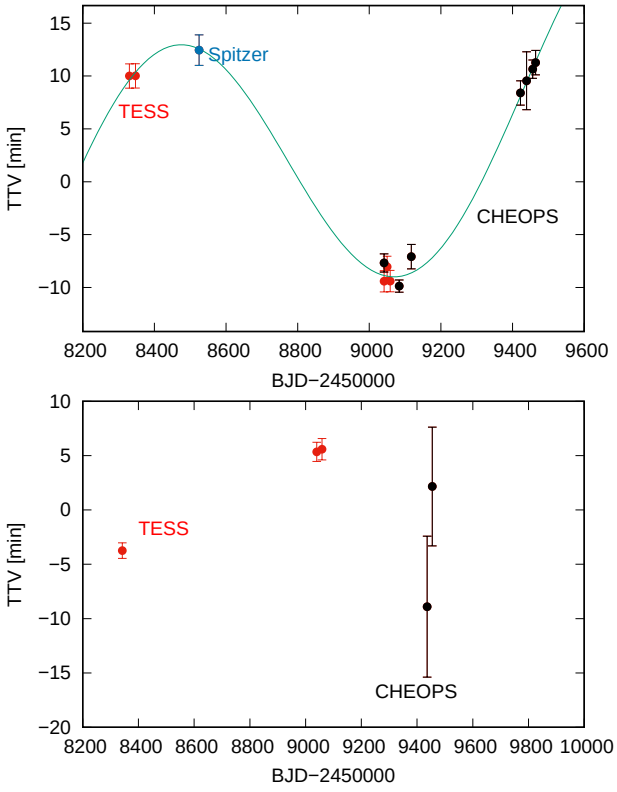

Fig. 3. TTV diagrams of AU Mic b (*upper panel*) calculated with T_c = 2 458 330.38416 and P_{mean} = 8.4631427 d, and AU Mic c (*lower panel*) calculated with T_c = 9454.8973 and P_{mean} = 18.85882 d. We included TESS (red symbols), *Spitzer* (blue symbols), and CHEOPS (black symbols) measurements. The harmonic fit to AU Mic b data illustrates the most probable shape of a periodic TTV fitted to the data. This is shown to illustrate the trend of the distribution without any dynamical interpretation.

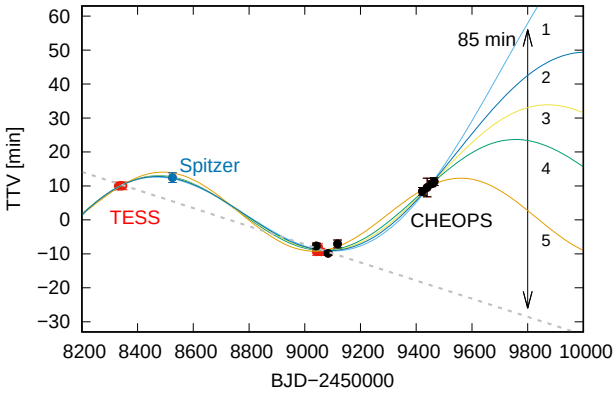

Fig. 4. Different predictions from the simplest harmonic TTV models to the 2022 opposition (colored curves) and the previously published linear ephemeris (gray dotted line). The colored curves fit equally well to all data points (see Table A.4 for their coefficients). Transits in 2022 August are expected to occur 40−85 min later than predictions prior to the CHEOPS 2021 observations.

and the linear terms in $O-C$: $c_1 = c_2 = 0$. (If there is no suspicion of a periodic TTV, linear epheremides (period and transit time) are given as $A = 0$ solutions of Eq. (1)). The currently available times of minima lead to T_c = 2 458 330.38416 ± 0.00005 d and P_{mean} = 8.4631427 ± 0.0000005 d in case of AU Mic b and T_c = 2 4594 54.8973 ± 0.0005 d and P_{mean} = 18.85882 ± 0.00005 d in case of AU Mic c. With this selection, the peak-to-peak amplitude of the TTV of AU Mic b and c are 23 and 9.5 min, respectively (Fig. 3).

The derived P_{mean} depends on which parts of the $O-C$ are constrained by data. It is likely that $P_{mean} \approx P_{orb}$, but, in general, equality cannot be guaranteed, in particular when the $O-C$ is sparsely sampled and with significant TTVs, as in the present case. The result is that the fitted coefficients c_1 and c_2 become uncertain. Despite the fact that T_c and P_{mean} were determined such that c_1 and c_2 vanish, they have error terms that correlate to the other parameters. The simplest form of an $O-C$ model describing a periodic process has all five free variables in the form of Eq. (1): A, P, and ϕ that are fitted, and c_1 and c_2 as parametrric constants determined from the data, which are therefore in correlation with the other three parameters.

The currently measured transits are concentrated in four relatively narrow windows (from a single transit to three-month observations) in the case of AU Mic b, and three similar windows in the case of AU Mic c. This leads to degeneracies in the best-fitting models of AU Mic b. Because of these degeneracies, we did not attempt to fit any curve to the current AU Mic c data.

The future transit times extrapolated from the modeled $O-C$ curves of AU Mic b are wildly diverging. The $O-C$ (determined as described above) and the possible $O-C$ predictions for the future (being equivalently well-fitting solutions of Eq. (1)) are plotted in Fig. 4 with curves, and the gray dashed line shows the predictions from the linear ephemeris based on previously published data. Transits predicted for 2022 are expected to occur 40−85 min later than expected without the 2021 observations of CHEOPS. We note that if the dominant process in the long-term behavior of AU Mic b is a period change with a constant rate, and the appropriate fit is a parabola instead of a harmonic function, the difference in transit time can be even more than 90 min. However, we think that this scenario is unlikely, because the position of the single measurement with the *Spitzer* telescope and the seemingly anticorrelated variations of the two planets in the system strongly suggest a periodic TTV in its leading term.

This TTV may reflect orbital changes. Ioannidis et al. (2016) suggested that starspots can also cause apparent TTVs of up to ≈1% of the transit duration. This would be on the order of 2 min in the case of AU Mic b. The observed effect is an order of magnitude larger than this prediction, and moreover with a pattern that is incompatible with the random behavior expected from stochastic spot occultations. Together, these findings strongly suggest an orbital dynamics origin of the TTVs.

The large TTVs of the AU Mic system are unusual, as can be seen when comparing to *Kepler* planets with confirmed TTVs (Fig. 5). Among the *Kepler* planets, only two that exhibit TTVs have shorter orbital periods than AU Mic b (Kepler-25 b and Kepler-1530 c, see Gajdoš et al. 2019). AU Mic b has a TTV semi-amplitude of $A \geq 11.5$ min, which is large in comparison to other planets with known TTVs. AU Mic c is still at the short-period end of the planets with known TTVs, while the semi-amplitude of the TTV is known with lower precision.

Martioli et al. (2021) estimate that the AU Mic b−c interactions lead to a superperiod of ≈82 days and significantly smaller amplitude than reported here. While we are certain that the TTV has its origin in the orbital physics, there are still too few data points to conclusively determine a superperiod or the possibility of a linear period drift in addition to the periodic TTV. These effects could point to either a currently ongoing migration or additional perturbing outer planets. To address these questions, a longer time-span of observed transit timings is required.

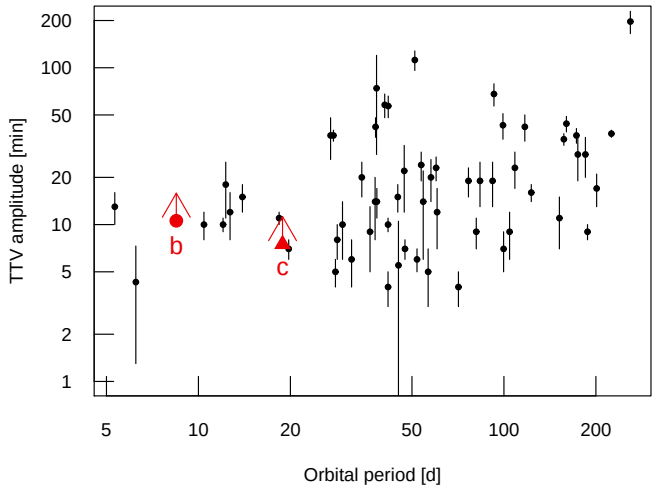

Fig. 5. Half-amplitude of periodic TTVs observed for *Kepler* planets (small dots) in comparison to the planets in the AU Mic system (red dot: AU Mic b, red triangle: AU Mic c). Due to the sparse coverage of observations, lower limits of TTV half-amplitudes are shown for AU Mic b and c.

4. Summary

In this Letter, we report our analysis of new CHEOPS observations of both planets in the AU Mic system and draw the following main conclusions:

1. AU Mic b shows very significant TTVs, with a minimum-to-maximum amplitude ≥23 min. AU Mic c shows TTVs with a minimum-to-maximum amplitude of ≥9.5 min. The best fitting mean orbital periods of AU Mic b and c are $P_{\rm mean} = 8.4631427 \pm 0.0000005$ d and $P_{\rm mean} = 18.85882 \pm 0.000005$ d, respectively. Taking the TTV into account, we predict that the transit times of AU Mic b in 2022 will happen 40−90 min later than expected from previously published linear ephemeris.
2. The transit depths of both planets are observed by CHEOPS to be smaller in 2021 than in 2020. The most likely reason is the increased activity of AU Mic with significant changes in the spot structure on the stellar surface.
3. Due to the large influence of spots on the size parameter $R_{\rm p}/R_\star$, its value should only be considered as a proxy for the actual sizes of the planets. A de-biased size determination requires detailed spot modeling with contemporary complementary observations, which we will address in a forthcoming paper.

The large-amplitude TTVs imply that the observations during the 2022 visibility have to be planned circumspectly. The ambiguity in transit-time predictions can be inaccurate up to 40−85 min which is about half of the transit duration. This can be especially critical for scheduling follow-up observations of either planet, for example with the *Hubble* Space Telescope or the *James Webb* Space Telescope.

Acknowledgements. CHEOPS is an ESA mission in partnership with Switzerland with important contributions to the payload and the ground segment from Austria, Belgium, France, Germany, Hungary, Italy, Portugal, Spain, Sweden, and the United Kingdom. The CHEOPS Consortium would like to gratefully acknowledge the support received by all the agencies, offices, universities, and industries involved. Their flexibility and willingness to explore new approaches were essential to the success of this mission. Gy.M.Sz. and Z.G. acknowledge the support of the Hungarian National Research, Development and Innovation Office (NKFIH) grant K-125015, a a PRODEX Experiment Agreement No. 4000137122 between the ELTE Eötvös Loránd University and the European Space Agency (ESA-D/SCI-LE-2021-0025), the Lendület LP2018-7/2021 grant of the Hungarian Academy of Science and the support of the city of Szombathely. Z.G. was supported by the VEGA grant of the Slovak Academy of Sciences No. 2/0031/22 and by the Slovak Research and Development Agency – the contract No. APVV-20-0148. A.Br. was supported by the SNSA. D.G. and L.M.S. gratefully acknowledge financial support from the Cassa di Risparmio di Torino (CRT) foundation under Grant No. 2018.2323 "Gaseous or rocky? Unveiling the nature of small worlds". A.C.C. and T.W. acknowledge support from STFC consolidated grant number ST/M001296/1. A.De. acknowledges support from the European Research Council (ERC) under the European Union's Horizon 2020 research and innovation programme (project FOUR ACES, grant agreement No. 724427), and from the National Centre for Competence in Research "PlanetS" supported by the Swiss National Science Foundation (SNSF). This work was also partially supported by a grant from the Simons Foundation (P.I. Queloz, grant number 327127). M.L. acknowledges support of the Swiss National Science Foundation under grant number PCEFP2_194576. G.Sc., G.Pi., I.Pa., L.Bo., R.Ra., and V.Na. and R.Ra. acknowledge the funding support from Italian Space Agency (ASI) regulated by "Accordo ASI-INAF n. 2013-016-R.0 del 9 luglio 2013 e integrazione del 9 luglio 2015 CHEOPS Fasi A/B/C". V.V.G. is an F.R.S.-FNRS Research Associate. Y.A. and M.J.H. acknowledge the support of the Swiss National Fund under grant 200020_172746. We acknowledge support from the Spanish Ministry of Science and Innovation and the European Regional Development Fund through grants ESP2016-80435-C2-1-R, ESP2016-80435-C2-2-R, PGC2018-098153-B-C33, PGC2018-098153-B-C31, ESP2017-87676-C5-1-R, MDM-2017-0737 Unidad de Excelencia Maria de Maeztu-Centro de Astrobiología (INTA-CSIC), as well as the support of the Generalitat de Catalunya/CERCA programme. The MOC activities have been supported by the ESA contract No. 4000124370. S.C.C.B. acknowledges support from FCT through FCT contracts nr. IF/01312/2014/CP1215/CT0004. X.B., S.C., D.G., M.F. and J.L. acknowledge their role as ESA-appointed CHEOPS science team members. This project was supported by the CNES. The Belgian participation to CHEOPS has been supported by the Belgian Federal Science Policy Office (BELSPO) in the framework of the PRODEX Program, and by the University of Liège through an ARC grant for Concerted Research Actions financed by the Wallonia-Brussels Federation. This work was supported by FCT – Fundação para a Ciência e a Tecnologia through national funds and by FEDER through COMPETE2020 – Programa Operacional Competitividade e Internacionalizacão by these grants: UID/FIS/04434/2019, UIDB/04434/2020, UIDP/04434/2020, PTDC/FIS-AST/32113/2017 and POCI-01-0145-FEDER-032113, PTDC/FIS-AST/28953/2017 and POCI-01-0145-FEDER-028953, PTDC/FIS-AST/28987/2017 and POCI-01-0145-FEDER-028987, O.D.S.D. is supported in the form of work contract (DL 57/2016/CP1364/CT0004) funded by national funds through FCT. B.-O.D. acknowledges support from the Swiss National Science Foundation (PP00P2-190080). This project has received funding from the European Research Council (ERC) under the European Union's Horizon 2020 research and innovation programme (project FOUR ACES grant agreement No 724427). It has also been carried out in the frame of the National Centre for Competence in Research PlanetS supported by the Swiss National Science Foundation (SNSF). D.E. acknowledges financial support from the Swiss National Science Foundation for project 200021_200726. L.D. is an F.R.S.-FNRS Postdoctoral Researcher. M.F. and C.M.P. gratefully acknowledge the support of the Swedish National Space Agency (DNR 65/19, 174/18). M.G. is an F.R.S.-FNRS Senior Research Associate. S.H. gratefully acknowledges CNES funding through the grant 837319. K.G.I. is the ESA CHEOPS Project Scientist and is responsible for the ESA CHEOPS Guest Observers Programme. She does not participate in, or contribute to, the definition of the Guaranteed Time Programme of the CHEOPS mission through which observations described in this Letter have been taken, nor to any aspect of target selection for the programme. This work was granted access to the HPC resources of MesoPSL financed by the Region Ile de France and the project Equip@Meso (reference ANR-10-EQPX-29-01) of the programme Investissements d'Avenir supervised by the Agence Nationale pour la Recherche. P.M. acknowledges support from STFC research grant number ST/M001040/1. Acknowledges support from the Spanish Ministry of Science and Innovation and the European Regional Development Fund through grant PGC2018-098153-B-C33, as well as the support of the Generalitat de Catalunya/CERCA programme. S.G.S. acknowledges support from FCT through FCT contract nr. CEECIND/00826/2018 and POPH/FSE (EC).

References

Benz, W., Broeg, C., Fortier, A., et al. 2021, Exp. Astron., 51, 109
Csizmadia, S. 2020, MNRAS, 496, 4442
Gaia Collaboration (Brown, A. G. A., et al.) 2018, A&A, 616, A1
Gajdoš, P., Vaňko, M., & Parimucha, Š. 2019, Res. Astron. Astrophys., 19, 041

Gilbert, E. A., Barclay, T., Quintana, E. V., et al. 2021, AJ, submitted [arXiv:2109.03924]
Hoyer, S., Guterman, P., Demangeon, O., et al. 2020, A&A, 635, A24
Ioannidis, P., Huber, K. F., & Schmitt, J. H. M. M. 2016, A&A, 585, A72
Kiraga, M. 2012, Acta Astron., 62, 67
Lithwick, Y., Xie, J., & Wu, Y. 2012, ApJ, 761, 122
Mamajek, E. E., & Bell, C. P. M. 2014, MNRAS, 445, 2169
Martioli, E., Hébrard, G., Correia, A. C. M., Laskar, J., & Lecavelier des Etangs, A. 2021, A&A, 649, A177
Maxted, P. F. L., & Gill, S. 2019, A&A, 622, A33
Maxted, P. F. L., Ehrenreich, D., Wilson, T. G., et al. 2021, MNRAS, in press [arXiv:2111.08828]
Miret-Roig, N., Galli, P. A. B., Brandner, W., et al. 2020, A&A, 642, A179
Oshagh, M., Santos, N. C., Boisse, I., et al. 2013, A&A, 556, A19
Plavchan, P., Barclay, T., Gagné, J., et al. 2020, Nature, 582, 497
Ricker, G. R., Winn, J. N., Vanderspek, R., et al. 2014, in Space Telescopes and Instrumentation 2014: Optical, Infrared, and Millimeter Wave, eds. J. Oschmann, M. Jacobus, M. Clampin, G. G. Fazio, & H. A. MacEwen, SPIE Conf. Ser., 9143, 914320
Sousa, S. G., Adibekyan, V., Delgado-Mena, E., et al. 2018, A&A, 620, A58
Szabó, G. M., Gandolfi, D., Brandeker, A., et al. 2021, A&A, 654, A159
Torres, C. A. O., Quast, G. R., da Silva, L., et al. 2006, A&A, 460, 695

[1] ELTE Eötvös Loránd University, Gothard Astrophysical Observatory, Szent Imre h. u. 112, 9700 Szombathely, Hungary
e-mail: szgy@gothard.hu
[2] MTA-ELTE Exoplanet Research Group, Szent Imre h. u. 112, 9700 Szombathely, Hungary
[3] Astronomical Institute, Slovak Academy of Sciences, 05960 Tatranská Lomnica, Slovakia
[4] Department of Astronomy, Stockholm University, AlbaNova University Center, 10691 Stockholm, Sweden
[5] Dipartimento di Fisica, Universita degli Studi di Torino, Via Pietro Giuria 1, 10125 Torino, Italy
[6] Centre for Exoplanet Science, SUPA School of Physics and Astronomy, University of St Andrews, North Haugh, St Andrews KY16 9SS, UK
[7] Observatoire Astronomique de l'Université de Genève, Chemin Pegasi 51, Versoix, Switzerland
[8] Physikalisches Institut, University of Bern, Gesellsschaftstrasse 6, 3012 Bern, Switzerland
[9] Center for Space and Habitability, Gesellsschaftstrasse 6, 3012 Bern, Switzerland
[10] Cavendish Laboratory, JJ Thomson Avenue, Cambridge CB3 0HE, UK
[11] INAF, Osservatorio Astronomico di Padova, Vicolo dell'Osservatorio 5, 35122 Padova, Italy
[12] Institut d'Astrophysique de Paris, UMR 7095 CNRS, Université Pierre & Marie Curie, 98 Bis Blvd. Arago, 75014 Paris, France
[13] Aix Marseille Univ., CNRS, CNES, LAM, 38 Rue Frédéric Joliot-Curie, 13388 Marseille, France
[14] Space Sciences, Technologies and Astrophysics Research (STAR) Institute, Université de Liège, Allée du 6 Août 19C, 4000 Liège, Belgium
[15] Instituto de Astrofisica de Canarias, 38200 La Laguna, Tenerife, Spain
[16] Departamento de Astrofisica, Universidad de La Laguna, 38206 La Laguna, Tenerife, Spain
[17] Institut de Ciencies de l'Espai (ICE, CSIC), Campus UAB, Can Magrans s/n, 08193 Bellaterra, Spain
[18] Institut d'Estudis Espacials de Catalunya (IEEC), 08034 Barcelona, Spain
[19] ADMATIS, 5. Kandó Kálmán Street, 3534 Miskolc, Hungary
[20] Depto. de Astrofisica, Centro de Astrobiologia (CSIC-INTA), ESAC Campus, 28692 Villanueva de la Cañada, Madrid, Spain
[21] Instituto de Astrofisica e Ciencias do Espaco, Universidade do Porto, CAUP, Rua das Estrelas, 4150-762 Porto, Portugal
[22] Departamento de Fisica e Astronomia, Faculdade de Ciencias, Universidade do Porto, Rua do Campo Alegre, 4169-007 Porto, Portugal
[23] Space Research Institute, Austrian Academy of Sciences, Schmiedlstrasse 6, 8042 Graz, Austria
[24] Université Grenoble Alpes, CNRS, IPAG, 38000 Grenoble, France
[25] Institute of Planetary Research, German Aerospace Center (DLR), Rutherfordstrasse 2, 12489 Berlin, Germany
[26] Université de Paris, Institut de Physique du Globe de Paris, CNRS, 75005 Paris, France
[27] Centre for Mathematical Sciences, Lund University, Box 118, 221 00 Lund, Sweden
[28] Astrobiology Research Unit, Université de Liège, Allée du 6 Août 19C, 4000 Liège, Belgium
[29] Leiden Observatory, University of Leiden, PO Box 9513, 2300 RA Leiden, The Netherlands
[30] Department of Space, Earth and Environment, Chalmers University of Technology, Onsala Space Observatory, 43992 Onsala, Sweden
[31] University of Vienna, Department of Astrophysics, Türkenschanzstrasse 17, 1180 Vienna, Austria
[32] Department of Physics, University of Warwick, Gibbet Hill Road, Coventry CV4 7AL, UK
[33] Science and Operations Department – Science Division (SCI-SC), Directorate of Science, European Space Agency (ESA), European Space Research and Technology Centre (ESTEC), Keplerlaan 1, 2201 AZ Noordwijk, The Netherlands
[34] Konkoly Observatory, Research Centre for Astronomy and Earth Sciences, Konkoly Thege Miklós út 15-17, 1121 Budapest, Hungary
[35] IMCCE, UMR 8028 CNRS, Observatoire de Paris, PSL Univ., Sorbonne Univ., 77 Av. Denfert-Rochereau, 75014 Paris, France
[36] Astrophysics Group, Keele University, Staffordshire ST5 5BG, UK
[37] Department of Astrophysics, University of Vienna, Tuerkenschanzstrasse 17, 1180 Vienna, Austria
[38] INAF, Osservatorio Astrofisico di Catania, Via S. Sofia 78, 95123 Catania, Italy
[39] Institute of Optical Sensor Systems, German Aerospace Center (DLR), Rutherfordstrasse 2, 12489 Berlin, Germany
[40] Dipartimento di Fisica e Astronomia "Galileo Galilei", Universita degli Studi di Padova, Vicolo dell'Osservatorio 3, 35122 Padova, Italy
[41] ESTEC, European Space Agency, 2201 AZ Noordwijk, The Netherlands
[42] Center for Astronomy and Astrophysics, Technical University Berlin, Hardenberstrasse 36, 10623 Berlin, Germany
[43] Institut für Geologische Wissenschaften, Freie Universität Berlin, 12249 Berlin, Germany
[44] Space Science Data Center, ASI, Via del Politecnico snc, 00133 Roma, Italy
[45] INAF, Osservatorio Astronomico di Roma, Via Frascati 33, 00078 Monte Porzio Catone, RM, Italy
[46] Institute of Astronomy, University of Cambridge, Madingley Road, Cambridge CB3 0HA, UK
[47] ELTE Eötvös Loránd University, Institute of Physics, Pázmány Péter Sétány 1/A, 1117 Budapest, Hungary

Appendix A: Data tables

In this appendix, we present tables with detailed parameters used in the transit fitting, as cited in the main text.

Table A.1. Priors and posteriors on planet parameters. We note that P_i refers to the instantaneous period that best fits the 2021 measurements, and is different from $P_{\rm mean}$, which minimizes the scatter of the TTVs of all observations between 2018–2021.

	AU Mic b	AU Mic c
	PRIORS	
D	$\mathcal{N}(0.003, 0.001)$	$\mathcal{N}(0.0015, 0.0004)$
$W[h]$	$\mathcal{N}(3.656, 0.203)$	$\mathcal{N}(3.892, 0.4)$
b	$\mathcal{U}(0.00, 0.30)$	$\mathcal{U}(0.3, 0.7)$
$P_i[d]$	$\mathcal{N}(8.463000, 0.003)$	$\mathcal{N}(18.8590, 0.0030)$
T_0	$\mathcal{N}(9447.52630, 0.004)$	$\mathcal{N}(9436.0350, 0.0072)$
	POSTERIORS	
D	0.00187 ± 0.00008	0.00098 ± 0.00010
$W[h]$	3.514 ± 0.026	4.290 ± 0.307
b	0.17 ± 0.10	0.58 ± 0.13
$P_i[d]$	8.46353 ± 0.00024	18.8602 ± 0.0026
T_0	9447.52634 ± 0.00046	9436.036 ± 0.004

Table A.2. Observed mid-transit times and $O - C$ values of AU Mic b based on *TESS*, Spitzer, and *CHEOPS* observations analyzed in the present work, with T_c = 2 458 330.38416 d and $P_{\rm mean}$ = 8.4631427 d. References to transit times are: *a*: Szabó et al. (2021), *b*: Plavchan et al. (2020), *c*: This Letter.

Designation	Transit Time [BJD−2 450 000]	$O - C$ [min]	Err [min]
TESS S1#1[a]	8330.3911±0.0009	10.00	1.33
TESS S1#2[a]	8347.3174±0.0009	10.02	1.33
Spitzer#1[b]	8525.04509±0.0010	12.45	1.43
TESS S27#1[a]	9041.2816±0.0008	-9.42	1.17
TESS S27#2[a]	9049.7457±0.0008	-8.05	1.17
TESS S27#3[a]	9058.2080±0.0008	-9.40	1.17
CHEOPS 20-07-10[a]	9041.2828±0.0006	-7.70	0.87
CHEOPS 20-08-21[a]	9083.5970±0.0004	-9.88	0.58
CHEOPS 20-09-24[a]	9117.4515±0.0008	-7.08	1.17
CHEOPS 21-07-26[c]	9422.1342±0.0010	8.40	1.43
CHEOPS 21-08-12[c]	9439.0636±0.0021	9.55	3.15
CHEOPS 21-08-29[c]	9455.9895±0.0007	10.65	1.0
CHEOPS 21-09-06[c]	9464.4531±0.0009	11.25	1.27

Table A.3. Observed mid-transit times and $O - C$ values of AU Mic c based on *TESS* and *CHEOPS* observations analyzed in the present work, with T_c = 2 459 454.8973 d and $P_{\rm mean}$ = 18.85882 d. References to transit times are: *a*: Gilbert et al. (2021), *b*: This Letter.

Designation	Transit Time [BJD−2 450 000]	O-C [min]	Err [min]
TESS S1#1[a]	8342.22432±0.0004	-3.75	0.71
TESS S27#1[a]	9040.00697±0.0005	5.34	0.88
TESS S27#2[a]	9058.86596±0.0006	5.58	0.98
CHEOPS 21-08-09[b]	9436.0323±0.0045	-8.90	6.48
CHEOPS 21-08-28[b]	9454.8988±0.0038	2.16	5.47

A.1. Coefficients of the model curves in Fig. 4

In this subsection, we give the coefficients of the model curves in Fig. 4. The purpose of this table is to enable the reproduction of the figure. The coefficients refer to time measured in BJD-2 450 000 days. We emphasize that we do not attribute any physical interpretation to these fits. Moreover, the various fits are equally consistent with the current data.

The equation of the model curves is equivalent to Eq. 1, but has a different parametrization to reduce parameter correlations and give more stable fits. The fitted curves use the following parametric function:

$$C(t) = a_0 \sin(a_1[t - a_2]) + a_3(t - a_2) + a_4, \quad \text{(A.1)}$$

where the coefficients are listed in Table A.4.

Table A.4. Coefficients of the model curves in Fig. 4.

Curve designation	Coefficients				
	a_0	a_1	a_2	a_3	a_4
1	13.57	0.0049061	9410.9	0.00833	−2.657
2	29.18	0.0033930	9709.9	0.04665	34.921
3	11.18	0.0058742	9296.77	−0.00016	−8.469
4	15.85	0.0044917	9475.23	0.01502	2.442
5	19.18	0.0040833	9548.96	0.02380	10.170

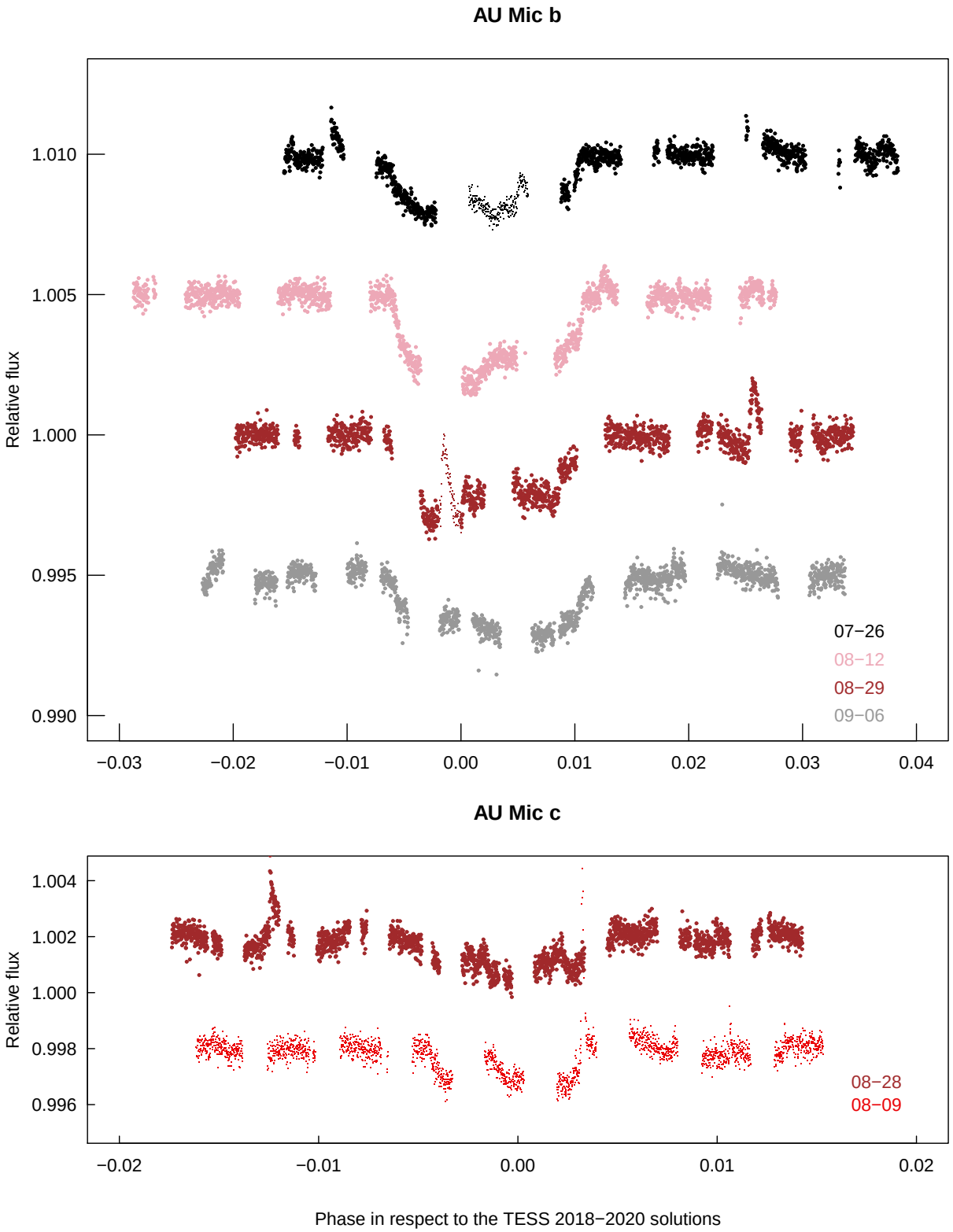

Fig. A.1. *CHEOPS* observations of AU Mic b (upper panel) and AU Mic c (lower panel) transits analyzed in this Letter. The 21-07-26 and 21-08-29 transits of AU Mic b were contaminated by flares. These points have been omitted from light curve fitting (plotted here with smaller dots). The labels show the date of the start of the visits in MM-DD format. The pixel/flux scale of the two panels is equal in order to show the relative amplitudes of the two planets.